Article

Not peer-reviewed version

Development of a Novel Controller for Brushless DC Motor Drive Systems Combining Decision Tree and Sliding Mode Theory

Kuei-Hsiang Chao *, Yu-Hong Guo, Chin-Tsung Hsieh

Posted Date: 30 April 2026

doi: 10.20944/preprints202604.2195.v1

Keywords: brushless DC motor; field-oriented control; decision tree theory; sliding mode controller; extension theory; exponential reaching law; constant speed reaching law

 doi:10.20944/preprints202604.2195.v1

Article

Development of a Novel Controller for Brushless DC Motor Drive Systems Combining Decision Tree and Sliding Mode Theory

Kuei-Hsiang Chao *, Yu-Hong Guo and Chin-Tsung Hsieh

Department of Electrical Engineering, National Chin-Yi University of Technology, Taichung 41170, Taiwan

* Correspondence: chaokh@ncut.edu.tw; Tel: +886-4-2392-4505 (ext.7272); Fax: +886-4-2392-2156

Abstract

This paper proposes a novel speed controller design for a brushless DC motor (BLDCM) under field-oriented control (FOC). The designed novel speed controller combines decision tree theory (DTT) and sliding mode theory (SMT). First, the regression algorithm of the classification and regression tree (CART) within decision tree theory is utilized to divide the speed error between the BLDCM's speed command and actual speed into 10 intervals. Based on this, three parameters of the existing exponential reaching law sliding mode controller (ERLSMC)—the sliding mode dynamic trajectory control gain, the exponential reaching gain, and the constant speed reaching gain—are configured. Next, the mean squared error (MSE) of each node after splitting is calculated to identify the root node. According to the selected split variable and splitting point, the data is divided into two subsets, and this process is repeated for each child node. Consequently, during the operation of the BLDCM, appropriate adjustments for the three gains can be provided to the sliding mode speed controller. Subsequently, a new sliding mode dynamic trajectory control gain is recalculated based on the rate of change of the speed error. This allows the overshoot in the system's speed response, caused by adopting the exponential reaching law (ERL), to be improved under different operating conditions through the modulation of its three gains. It also enables the speed response of the BLDCM drive system to rapidly track the speed command under various operating conditions. Therefore, the proposed control law involves no complex computations and does not require a massive amount of training data, making it easy to implement. Finally, Matlab/Simulink simulation software is used to simulate the application of the proposed control law to the BLDCM drive system. Its control performance is compared with sliding mode controllers (SMCs) utilizing three different reaching laws: the constant speed reaching law (CSRL), the ERL, and the extension theory combined with exponential reaching law (ETERL). The simulation results demonstrate that the proposed novel speed controller outperforms the SMCs with the other three reaching laws in terms of both speed command tracking and load regulation response.

Keywords: brushless DC motor; field-oriented control; decision tree theory; sliding mode controller; extension theory; exponential reaching law; constant speed reaching law

1. Introduction

In recent years, due to the rapid development of technology, the requirements for motor drive performance have increasingly risen; therefore, AC motors have also received significant attention. Among them, the brushless DC motor (BLDCM) [2] within permanent magnet synchronous motors [1] is widely chosen in industrial applications due to its advantages such as high torque, high torque-to-weight ratio, high efficiency, and low noise. However, as the requirements for speed response and position control precision have become increasingly stringent, field-oriented control (FOC) [3] technology is widely adopted in the industrial field to achieve precise speed and position control.

 doi:10.20944/preprints202604.2195.v1

Traditional FOC achieves a closed-loop system control through coordinate transformations and three proportional-integral (P-I) controllers [4]: a speed controller, a *d*-axis controller, and a *q*-axis controller. However, although the traditional P-I controller is relatively easy to design, it not only fails to simultaneously balance command tracking and load regulation responses, but its control performance also degrades when the system is subjected to disturbances. Furthermore, different control laws have their respective unresolvable issues. For instance, while the traditional sliding mode controller (SMC) [5] possesses strong anti-interference capabilities, it cannot balance command tracking and load regulation responses. Fuzzy logic theory (FLT) is applicable to various fields due to its ease of design and strong robustness against disturbances; however, it suffers from overly lengthy computation times. Moreover, because it solves problems through approximation, its performance may be insufficient for systems requiring high control precision, such as highly nonlinear systems or those needing fast dynamic responses. As for extension theory (ET) [6], although it can flexibly adjust system parameters to meet different dynamic performance control requirements, there are concerns about system instability if operating points fall outside the neighborhood domain. The two-degree-of-freedom controller (2DOFC) enhances overall control performance by combining a feedforward controller and a P-I controller; due to its design that separates target tracking and disturbance rejection, it features high flexibility and is suitable for complex control demands. Nevertheless, the parameters of this controller are difficult to design and tune, which is not only time-consuming but also inefficient. While decision tree theory (DTT) involves simple calculations, it is more suitable for linear problems such as classification and regression. For more complex nonlinear problems, it is prone to producing erroneous results due to data perturbations or uncertainties. Therefore, it is necessary to introduce algorithms into the controller or combine different control laws to achieve adaptive capabilities [7] and further enhance control performance. Examples include combining FLT with a P-I controller [8], combining ET with an SMC [9], and combining extendable fuzzy theory (EFT) with a 2DOFC [10]. However, the combination of FLT and a P-I controller cannot fully achieve the expected control performance for both speed command tracking and load regulation responses. The controller combining ET and SMC exhibits a slight overshoot during minor speed increases in speed command tracking. Meanwhile, the EFT combined with a 2DOFC still presents slight oscillations in the recovery response during load regulation. Consequently, by combining DTT and sliding mode theory (SMT), this paper proposes a control method that can automatically adjust three variable parameters of the sliding mode controller under different operating conditions within the rated speed range, thereby improving system stability and achieving adaptive control performance.

The control law proposed in this paper uses the speed error between the speed command and the actual speed of the brushless DC motor as a feature. It utilizes the regression algorithm of the classification and regression tree (CART) from DTT to divide this feature into 10 intervals. Based on this, the individual parameters for the sliding mode dynamic trajectory control gain, the exponential reaching gain, and the constant speed reaching gain of the sliding mode controller applying the exponential reaching law are configured. Subsequently, the optimal splitting point is found through calculation to serve as the root node, and the data is divided into two parts based on the selected split variable and splitting point. This process is then repeated for each child node to construct the decision tree. Consequently, during the operation of the BLDCM, the appropriate variation amounts for the three gains of the sliding mode speed controller can be outputted. Then, a new sliding mode dynamic trajectory control gain is recalculated based on the rate of change of the speed error. This ensures that the overshoot generated in the system's speed command tracking response, which occurs when only the exponential reaching law is adopted, can be improved under different operating conditions. Finally, this paper uses simulation results to verify and compare the performance of the proposed speed controller with sliding mode controllers (SMCs) adopting three other reaching laws in terms of speed command tracking and load regulation responses.

 doi:10.20944/preprints202604.2195.v1

2. Brushless DC Motor Drive System

The primary difference between a BLDCM and a brushed DC motor (BDCM) lies in the commutation method. A BDCM relies on the mechanical contact between brushes and a commutator for commutation; as the rotor turns, the brushes continuously switch contact points, altering the current direction to generate a continuously rotating magnetic field. In contrast, a BLDCM employs an electronic commutation method. By integrating magnetic components such as Hall effect sensors or optical encoders [11] onto the rotor shaft, it detects and feeds back the rotor's position to the controller in real-time. This allows the controller to adjust the current direction in the stator windings based on the current rotor position, thereby maintaining a stable rotating magnetic field to drive the rotor and achieve commutation.

2.1. FOC Architecture of the BLDCM System

FOC is also known as vector control. Its purpose is to utilize coordinate transformations [12] to convert the voltage and flux equations of the BLDCM from a three-phase rotating coordinate system into a two-axis synchronous coordinate system. This simplifies the motor's mathematical model [13] and consequently reduces both the computational burden of the system and the complexity of the controller design. Its operational flow involves decoupling current signals into voltage signals via P-I controllers, followed by coordinate transformations. Therein, space vector pulse width modulation (SVPWM) technology is used to control the switching actions of the six power semiconductors within the inverter [14]. Subsequently, output parameters such as the motor's rotational speed, voltage, and current are fed back to the controller. Through the speed controller, speed command tracking is achieved, and steady-state error is eliminated.

In the two-axis synchronous rotating (d,q) coordinate system, if the rotor of the BLDCM has no damping winding and the permanent magnets are located on the rotor surface, the permanent magnets can be regarded as an equivalent current source. If the rotational speed of an arbitrary rotating reference frame ω is defined as the rotor speed, we can set $\omega = \omega_r$. Furthermore, since the electrical rotor speed of a synchronous motor is its synchronous speed, we have $\omega = \omega_r = \omega_e$; and because the rotor current is also the rotor current that generates the magnetic field, $i_r = I_{rF}$. Because the permanent magnets of the rotor only exist on the *d*-axis, they can be equivalently represented by a constant current source I_{rF} on the *d*-axis, while the *q*-axis rotor current is zero; therefore, the magnetic flux can be expressed as Equations (1) and (2).

$$\phi_{ds} = L_d i_{ds} + L_m I_{rF} \tag{1}$$

$$\phi_{qs} = L_q i_q \tag{2}$$

Where: ϕ_{ds} and ϕ_{qs} are the stator fluxes of the *d*-axis and *q*-axis, respectively, and the flux linkage generated by the permanent magnets in the stator windings is $L_m I_{rF} = L_m i_r = \phi_F$, thus the stator voltages can be expressed as Equations (3) and (4).

$$v_{ds} = R_s i_{ds} + L_d \frac{di_{ds}}{dt} - \omega_e L_q i_{qs} \tag{3}$$

$$v_{qs} = R_s i_{qs} + L_q \frac{di_{qs}}{dt} + \omega_e L_d i_{ds} + \omega_e \phi_F \tag{4}$$

Where: v_{ds} and v_{qs} are the stator voltages of the *d*-axis and *q*-axis, respectively, R_s is the stator resistance, i_{ds} and i_{qs} are the stator currents of the *d*-axis and *q*-axis, respectively, ω_e is the electrical angular velocity, and L_d and L_q are the stator inductances of the *d*-axis and *q*-axis, respectively. Because the *d*-axis is directly facing the stator windings, while the *q*-axis is directly facing the stator core, the magnetic reluctance of the *d*-axis will be greater than that of the *q*-axis, hence $L_d < L_q$.

 doi:10.20944/preprints202604.2195.v1

The motor's electromagnetic torque and mechanical equations can then be expressed as Equations (5) and (6).

$$T_e = \frac{3}{2}\frac{P}{2}[\phi_F i_{qs} + (L_d - L_q) i_{ds} i_{qs}] \tag{5}$$

$$T_e = \frac{P}{2} J \frac{d\omega_m}{dt} + T_L \tag{6}$$

Where: T_e is the electromagnetic torque, P is the number of poles, J is the moment of inertia, ω_m is the mechanical rotational speed, and T_L is the load torque.

If FOC is adopted, we can set $i_{ds} = 0$, which also simplifies Equations (3)-(5) to Equations (7)-(9).

$$v_{ds} = -\omega_e L_q i_{qs} \tag{7}$$

$$v_{qs} = R_s i_{qs} + L_q \frac{di_{qs}}{dt} + \omega_e \phi_F \tag{8}$$

$$T_e = \frac{3}{2}\frac{P}{2}\phi_F i_{qs} \tag{9}$$

From the relationship between the electromagnetic torque T_e and the q-axis stator current i_{qs} in Equation (9), the torque constant K_t can be expressed as Equation (10).

$$K_t = \frac{3}{2}\frac{P}{2}\phi_F \tag{10}$$

By substituting Equation (10) into the mechanical motion Equation of the BLDCM, it can be rearranged as Equation (11).

$$\frac{d\omega_m}{dt} = \frac{1}{J}\left(K_t i_{qs} - B\omega_m - T_L\right) \tag{11}$$

In the FOC method, coordinate transformations not only simplify the complexity of the equations but also convert time-varying variables into constant values. Therefore, by first aligning the d-axis of the two-axis stationary coordinate system with the q-axis of the three-phase stationary coordinate system, the Clarke transformation is utilized to convert the feedback three-phase (a,b,c) stationary coordinate AC currents of the motor into two-phase (α,β) stationary coordinate AC currents, as shown in Equation (12).

$$\begin{bmatrix} i_\alpha \\ i_\beta \end{bmatrix} = \begin{bmatrix} 1 & -1/2 & -1/2 \\ 0 & \sqrt{3}/2 & -\sqrt{3}/2 \end{bmatrix} \begin{bmatrix} i_a \\ i_b \\ i_c \end{bmatrix} \tag{12}$$

Then, the Park transformation is used to convert the (α,β) stationary coordinate AC currents into (d,q) synchronous coordinate DC currents, which are fed back into the controller; this transformation expression is shown as Equation (13).

$$\begin{bmatrix} i_d \\ i_q \end{bmatrix} = \begin{bmatrix} \cos\theta & \sin\theta \\ -\sin\theta & \cos\theta \end{bmatrix} \begin{bmatrix} i_\alpha \\ i_\beta \end{bmatrix} \tag{13}$$

The inverse Park transformation can convert the voltages in the (d,q) -axis synchronous rotating frame coordinates into AC voltages in the (α,β) stationary frame coordinates, as shown in Equation (14).

$$\begin{bmatrix} v_\alpha \\ v_\beta \end{bmatrix} = \begin{bmatrix} \cos\theta & -\sin\theta \\ \sin\theta & \cos\theta \end{bmatrix} \begin{bmatrix} v_d \\ v_q \end{bmatrix} \tag{14}$$

Subsequently, the voltages v_α and v_β generated through this transformation are used for SVPWM. Then, through its internal inverse Clarke transformation, the two-phase (α,β) AC voltages are converted into three-phase (a,b,c) AC voltages, thereby controlling the switching of the inverter; its transformation equation is shown as Equation (15).

 doi:10.20944/preprints202604.2195.v1

$$\begin{bmatrix} v_a \\ v_b \\ v_c \end{bmatrix} = \begin{bmatrix} 1 & 0 \\ -1/2 & \sqrt{3}/2 \\ -1/2 & -\sqrt{3}/2 \end{bmatrix} \begin{bmatrix} v_\alpha \\ v_\beta \end{bmatrix} \tag{15}$$

Through the above steps, the closed-loop control of the BLDCM system can be realized. From the torque and voltage equations, it can be observed that when FOC is adopted, controlling the *q*-axis current can control the magnitude of the torque, and the *d*-axis voltage is only related to the *q*-axis current. This further proves that for the system architecture of the BLDCM, this control method can effectively simplify and reduce the difficulty of its control.

2.2. P-I Controller

A P-I controller is a type of controller used to adjust the stability and response speed of a control system; it is widely used due to its simple architecture and ease of tuning. In the FOC system of a BLDCM, P-I controllers are typically used to regulate the closed-loop control of speed and current. In the current control of the *d* and *q* axes, the system converts the three-phase currents into the *d*-axis and *q*-axis stator currents i_{ds} and i_{qs}, and the P-I controllers perform closed-loop control on both respectively to achieve precise magnetic field and torque control. Generally, to maximize the motor torque, which is to achieve the maximum torque per ampere (MTPA) [15], $i_{ds} = 0$ is set, and the *q*-axis P-I controller adjusts the input based on the error between the current i_{qs} and the target value i_{qs}^*, thereby achieving precise torque control. Its target value is the torque current command i_{qs}^* generated by the speed loop P-I controller based on the error between the speed command and the actual speed. In this way, these three P-I controllers ensure that the motor's output meets the control requirements, enabling the system to achieve a relatively fast response and eliminate steady-state error.

Although the P-I controller is suitable for most control systems, it may lead to a decrease in control precision when dealing with nonlinear systems, and its response may also suffer from delay issues when facing rapid dynamic changes in the system. Therefore, this paper will replace the P-I controller in the speed loop with the proposed novel controller, thereby optimizing the performance of speed command tracking and load regulation responses. Figure 1 shows the block diagram of the FOC for the BLDCM.

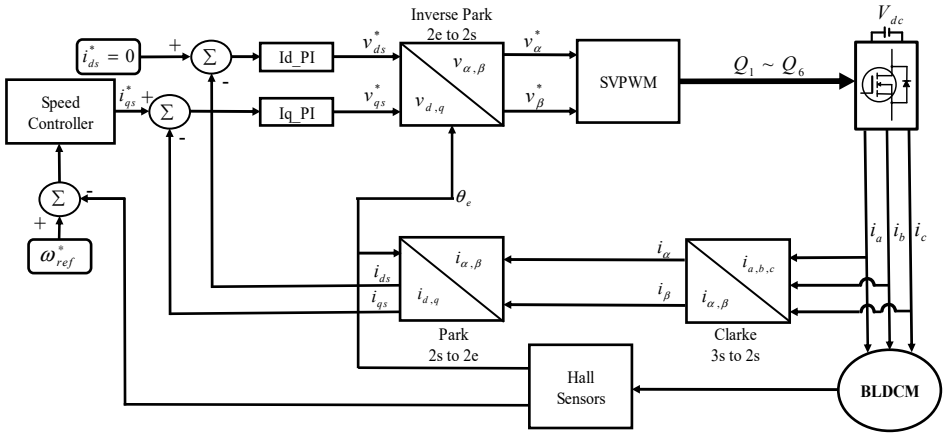

Figure 1. Block diagram of the FOC for the BLDCM.

 doi:10.20944/preprints202604.2195.v1

3. Novel Algorithm Based on Decision Tree Theory

If only a P-I controller is used for the speed loop controller in FOC, it will be difficult to simultaneously balance speed command tracking and load regulation performance. Therefore, this paper will replace the speed loop P-I controller with the proposed novel controller. The architecture of this controller combines DTT and SMT; through DTT, the variable parameters of the SMC are assigned corresponding values within set error intervals based on the error between the current rotational speed and the speed command, thereby achieving adjustable robust control [16] and thus improving overall control performance.

3.1. Decision Tree Theory

Decision tree is a classical machine learning and data mining method. Its core idea is to decompose the decision-making process through a tree-like structure, which is used to solve classification and regression problems. Its basic structure is divided into three parts: the root node (also known as the parent node), internal nodes (also known as split nodes), and leaf nodes (also known as child nodes). Among them, the root node is the starting point of the decision tree, each internal node represents a decision or split, and the leaf node is the endpoint of the decision tree, representing the final classification result or regression value. Figure 2 shows the architecture diagram of a decision tree.

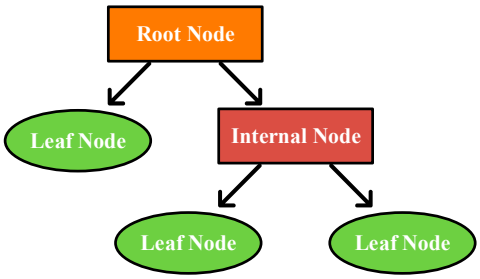

Figure 2. Decision tree architecture diagram.

The development of DTT primarily originates from the fields of statistics and artificial intelligence, with its history tracing back to the 1960s. Over time, it has evolved into algorithms suitable for various problems, such as ID3 (iterative dichotomiser 3), C4.5, CHAID (chi-squared automatic interaction detector), and CART (classification and regression trees) [17]. Among them, the ID3 algorithm uses entropy and information gain as splitting criteria and is only applicable to classification problems. C4.5 is an improved version of ID3; because it can handle continuous features, it is superior to the former. The CHAID algorithm splits based on chi-squared tests and is commonly used in marketing and behavioral analysis. The CART algorithm introduces the Gini index and mean squared error (MSE) or mean absolute error (MAE) as splitting criteria for classification trees and regression trees, respectively, making it a relatively common decision tree algorithm today.

3.1.1. Classification and Regression Trees Algorithm

The CART algorithm was proposed by Leo Breiman et al. in 1984 [17]. It systematically constructed the theory of decision trees through the CART model, encompassing algorithm frameworks for both classification and regression trees. By utilizing the Gini index and MSE or MAE as splitting criteria, it identifies the optimal splitting point (i.e., root node). Because it is applicable to both classification and regression problems, its scope of application is broader, making it a core foundation and a widely used method among modern decision tree algorithms.

In classification trees, CART uses the Gini index as the splitting criterion, as shown in Equation (16).

 doi:10.20944/preprints202604.2195.v1

$$Gini(t) = 1 - \sum_{i=1}^{C_n} p_i^2 \tag{16}$$

Where: p_i is the proportion of the *i*-th category in node *t*, and C_n is the number of categories.

The Gini gain, used to select the optimal splitting point, can be obtained from Equation (17).

$$\Delta Gini = Gini(t) - \left(\frac{N_{left}}{N} Gini(t_{left}) + \frac{N_{right}}{N} Gini(t_{right}) \right) \tag{17}$$

Where: t_{left} and t_{right} are the left child node and right child node respectively, N is the number of samples in node *t*, and N_{left} and N_{right} are the number of samples in the left and right child nodes, respectively.

In regression trees, CART uses MSE or MAE as the splitting criterion, as shown in Equations (18) and (19), respectively.

$$MSE(t) = \frac{1}{N} \sum_{i=1}^{N} (y_i - \hat{y})^2 \tag{18}$$

$$MAE(t) = \frac{1}{N} \sum_{i=1}^{N} |y_i - \hat{y}| \tag{19}$$

Where: y_i is the actual value of sample *i*, and $\hat{y}$ is the sample mean in the node (i.e., the average predicted value), which can be expressed as Equation (20).

$$\hat{y} = \frac{1}{N} (y_1 + y_2 + \ldots + y_N) \tag{20}$$

The $\Delta\mathrm{MSE}$ and $\Delta\mathrm{MAE}$ used to select the optimal splitting point are expressed as Equations (21) and (22), respectively.

$$\Delta MSE = MSE(t) - \left(\frac{N_{left}}{N} MSE(t_{left}) + \frac{N_{right}}{N} MSE(t_{right}) \right) \tag{21}$$

$$\Delta MAE = MAE(t) - \left(\frac{N_{left}}{N} MAE(t_{left}) + \frac{N_{right}}{N} MAE(t_{right}) \right) \tag{22}$$

Where: MAE is the mean absolute value of the error, so it is more tolerant of a small number of large errors, making it suitable for problems seeking stable predictions. MSE is the mean squared value of the error, thereby amplifying the impact of larger errors, so it can ensure the uniformity of data within each leaf node by minimizing the squared difference after splitting, making it suitable for situations where suppressing large errors is desired. Therefore, decision trees commonly use MSE as the splitting criterion in regression problems.

3.1.2. Pruning

The pruning technique of decision trees is a method for model optimization; its main purpose is to reduce overfitting and improve the model's generalization ability. During the generation process of a decision tree, it is easy to generate a complex structure, making it perform well on training data but potentially overfit on unknown data. Therefore, pruning techniques are used to trim the decision tree after it is constructed to reduce unnecessary branches, thereby simplifying the model. The methods are mainly divided into pre-pruning and post-pruning [18]. Among them, pre-pruning stops the partitioning early during the tree building process; by setting limits to decide whether to continue branching, it stops expanding nodes when the branches cannot meet the conditions, preventing the tree from becoming overly complex. Post-pruning, on the other hand, first generates a complete decision tree, and then trims it from the bottom up, deleting branches that contribute less to the model. It commonly uses cross-validation or evaluates accuracy to confirm whether to prune, ensuring reduced error and enhanced generalization ability.

 doi:10.20944/preprints202604.2195.v1

3.1.3. Generation Principle of Regression Trees

The basic idea of a decision tree is to progressively split the sample space based on the different values of features to form a tree structure, where each internal node represents a feature, and each branch represents a different value of that feature. This splitting continues until each leaf node contains only one category or meets certain stopping criteria. The regression tree is specifically used for predicting continuous variables, so it is more suitable for motor speed control compared to the classification tree. Its main purpose is to partition the data space so that the relationship between the target variable (i.e., output) on each leaf node and the input variables can be best represented; the construction process of a regression tree is explained as follows:

Step 1: Calculate the MSE reduction value for each feature and splitting point according to the splitting criterion, and select the splitting point corresponding to the maximum reduction value.

Step 2: Split the dataset into two parts based on the selected splitting point using a dichotomous method.

Step 3: Repeat the above steps for each child node until the stopping condition is met.

Step 4: To prevent overfitting, the generated regression tree can be pruned.

3.2. Sliding Mode Controller

Generally speaking, traditional P-I controllers can meet the control performance requirements for most specific operating points. However, because the BLDCM is a highly coupled, nonlinear multivariable system, and system parameter variations, load changes, and external disturbances frequently occur, the originally anticipated control performance cannot be maintained, making it difficult to meet the control performance requirements of the application. Therefore, to improve this problem, many intelligent control laws have been used to directly replace traditional P-I controllers, or by combining different control laws, the controller is endowed with robustness or self-adaptive capabilities.

The variable structure control of the SMC has lower dependency on the motor model. Through the design of the sliding mode dynamic trajectory, the nonlinear dynamics of the system are transformed into linear dynamics on the sliding surface, providing it with strong anti-interference capabilities and robustness. It has high tolerance for system uncertainties and external disturbances, which yields good control effects for applications requiring high dynamic performance, such as BLDCM control.

3.2.1. State Variable Design

To use the SMC to replace the P-I controller in the traditional field-oriented speed control loop for speed loop control applications, a control strategy of $i_d = 0$ must be adopted. Therefore, Equation (23) can be derived from the d-q axis mathematical equations of the BLDCM in Equations (3) and (4). If the system is assumed to be ideal, the viscous friction coefficient can be ignored; thus, the equations of motion for the BLDCM in Equations (10) and (11) can be simplified to Equation (24).

$$\frac{di_{qs}}{dt} = \frac{1}{L_q}(-R_s i_{qs} - \frac{P}{2}\omega_m \phi_F + v_{qs}) \tag{23}$$

$$\frac{d\omega_m}{dt} = \frac{1}{J}(-T_L + \frac{3P}{4}\phi_F i_{qs}) \tag{24}$$

For speed tracking control, it is necessary to make the speed error (i.e., error value) between the controller's input signal the speed command ω_m^* and the actual feedback speed signal ω_m reach 0, meaning $\omega_m^* - \omega_m = 0$, and make the rate of change of the speed error $\dot{\omega}_m$ also 0, while the controller's output is the *q*-axis command current i_q^*. Therefore, the state variables of the BLDCM system can be expressed as Equation (25).

$$\begin{cases} x_1 = \omega_m^* - \omega_m \\ x_2 = \dot{x}_1 = -\dot{\omega}_m \end{cases} \tag{25}$$

 doi:10.20944/preprints202604.2195.v1

From the differentiation of Equations (24) and (25), the rate of change of the state variables can be derived, as shown in Equations (26).

$$\begin{cases} \dot{x}_1 = -\dot{\omega}_m = \dfrac{1}{J}(T_L - \dfrac{3P}{4}\phi_F i_{qs}) \\ \dot{x}_2 = -\ddot{\omega}_m = -\dfrac{1}{J}\left(\dfrac{3P}{4}\phi_F i_{qs}\right) \end{cases} \tag{26}$$

Let $D = \dfrac{1}{J}\left(\dfrac{3P}{4}\dfrac{L_m}{L_r}\phi_r\right)$, and substituting this into Equation (26) yields equation (27).

$$\dot{x}_2 = -\ddot{\omega}_m = -\frac{1}{J}\left(\frac{3P}{4}\phi_F i_{qs}\right) = -Di_{qs} \tag{27}$$

3.2.2. Sliding Mode Dynamic Trajectory Design

The operating principle of the SMC is to drive the system to move along a sliding mode dynamic trajectory (i.e., the sliding surface, which is referred to as a sliding line in this two-dimensional application). The sliding line function [19] can be expressed in the form of Equation (28).

$$s = cx_1 + x_2 \tag{28}$$

Where: s is the sliding line function, c is the sliding line control gain, and x_1, x_2 are the state variable functions.

To ensure the system reaches stability, it is required that $x_1 = 0$ and $x_2 = 0$. When $s(x_1, x_2) = 0$, let $x_2 = \dot{x}_1$, which results in $cx_1 + x_2 = cx_1 + \dot{x}_1 = 0$. From this, x_1 and x_2 can be solved, as shown in Equation (29).

$$\begin{cases} x_1 = x_1(0)e^{-ct} \\ x_2 = -cx_1(0)e^{-ct} \end{cases} \tag{29}$$

It can be seen from this that over time, both state variable x_1 and state variable x_2 will change at an exponential rate and eventually decay to 0. Therefore, $s = 0$ represents the designed sliding line; when the sliding line function is designed as $s = cx_1 + x_2$, after reaching the sliding line $s = 0$, the system's state variables will approach 0, thereby achieving the goal of state variable control.

3.2.3. Sliding Mode Reaching Law Design

To guarantee that the sliding line function s equals 0 at a certain point in time (i.e., reaches the sliding line) and remains stable, a reaching law function [20] must be designed. From the sliding line design, it is known that to make $s = 0$, the control effort function u must be designed to meet the control requirements. Thus, Equation (28) can be rewritten as Equation (30).

$$\dot{s} = c\dot{x}_1 + \dot{x}_2 = cx_2 + \dot{x}_2 = cx_2 - Di_{qs} \tag{30}$$

Since the output of the controller is i_{qs}^*, which is the q-axis reference current, we can set the control effort function to $u = i_{qs}$, allowing Equation (30) to be rewritten as Equation (31).

$$\dot{s} = cx_2 - Du \tag{31}$$

Where: $\dot{s}$ is the reaching law function.

According to Lyapunov's second method for stability [21], if a continuous function V exists, it must satisfy the following three conditions.

$$\begin{aligned} &(1) V(0) = 0 \\ &(2) V(s) > 0, s \neq 0 \\ &(3) \dot{V}(s) < 0, s \neq 0 \end{aligned} \tag{32}$$

 doi:10.20944/preprints202604.2195.v1

Therefore, if the system is stable at the equilibrium point $s=0$, it guarantees that $\lim_{t\to\infty} s(t)=0$. Furthermore, if we set $V=\frac{1}{2}s^2$, it not only satisfies conditions (1) and (2) in Equation (32) but also allows the third condition to be determined through analysis, as shown in Equation (33).

$$\dot{V}(x)=s\dot{s} \tag{33}$$

Through the derivation of the above formulas and the subsequent design of the reaching law function $\dot{s}$, we ensure that $\dot{V}(x)=s\dot{s}<0$. Common reaching laws include the constant speed reaching law and the exponential reaching law. The constant speed reaching law and the exponential reaching law can be expressed by Equations (34) and (35), respectively.

Constant speed reaching law:

$$\dot{s}=-\varepsilon\,\mathrm{sgn}(s),\varepsilon>0 \tag{34}$$

Exponential reaching law:

$$\dot{s}=-\varepsilon\,\mathrm{sgn}(s)-qs,\varepsilon>0,q>0 \tag{35}$$

Where: ε is the constant speed reaching gain, q is the exponential reaching gain, and $\mathrm{sgn}(s)$ is a sign function, as shown in Equation (36).

$$\mathrm{sgn}(s)=\begin{cases}1, & s>0\\ -1, & s<0\end{cases} \tag{36}$$

Based on the two reaching laws mentioned above, the expression for the controller u can be obtained. For $\dot{s}=-\varepsilon\,\mathrm{sgn}(s),\varepsilon>0$, we have $u=-cx_2-\varepsilon\,\mathrm{sgn}(s)$, which applies the control effort u to the motor model. The $-qs$ term of the exponential reaching law causes the value of the sliding line function s to decay exponentially over time. Therefore, to solve for $\dot{s}=-qs$, the general solution formula for a first-order linear differential equation can be utilized. This first-order linear differential Equation is:

$$\dot{s}+q(t)s=Q(t) \tag{37}$$

Applying the general solution formula to Equation (37) yields Equation (38).

$$s=e^{-\int q(t)dt}\left[\int Q(t)e^{\int q(t)dt}dt+C\right] \tag{38}$$

Where: C is the constant of integration.

To achieve $\dot{s}=-qs,q>0,\dot{s}+qs=0$, substitute $Q(t)=0$ into Equation (38) to obtain Equation (39).

$$s=e^{-\int qdt}\left[\int 0dt+C\right]=Ce^{-qt} \tag{39}$$

Wherein, since $s(0)$ is the initial value at $t=0$, setting $s(0)=C$ yields the final solution:

$$s(t)=s(0)e^{-qt} \tag{40}$$

From the above solution, it can be seen that the exponential decay term ($-qs$) in the exponential reaching law will cause the system to converge exponentially to the sliding line, and it automatically decelerates upon approaching, thereby reducing the chattering phenomenon in sliding mode control, which is equivalent to implicitly incorporating an integrator.

In summary, in the design steps of the SMC, the sliding line is first designed according to the state equations of the controlled object. Once the sliding line is reached, the stable state is achieved through exponential reaching. Then, the reaching law function $\dot{s}$ is designed to obtain the expression of the controller, and the Lyapunov stability criterion is used as the basis for the output response stability to ensure $s=0$, thereby achieving the final response result.

 doi:10.20944/preprints202604.2195.v1

3.2.4. Controller Output Design

According to the above reaching law design, the first two conditions of the Lyapunov function can guarantee $\lim_{t\to\infty} s(t)=0$. However, if the constant speed reaching law of Equation (34) is adopted, whether at $t=1s$ or $t=100s$, $s=0$ (i.e., reaching the sliding line) can satisfy the requirements of the Lyapunov function. But because its response speed is a constant value, it is similar to a traditional P-I controller and cannot simultaneously balance speed tracking and load regulation responses, making its practicality somewhat insufficient in actual applications. From Equation (35), it can be observed that the exponential reaching law possesses an integrator characteristic that the constant speed reaching law lacks. Furthermore, when approaching the sliding line (i.e., the value of the exponential reaching term is small), $\dot{s}=-qs$ approaches 0, so it is dominated by $-\varepsilon\,\mathrm{sgn}(s)$; conversely, if the distance is far greater than the sliding line (i.e., the value of s is large), the value of $\dot{s}=-qs$ will also be large, and at this time, it is dominated by the exponential reaching term. This improves the speed response of reaching the sliding line, enabling the system to approach the sliding line at a faster speed. Therefore, when setting parameters, q (exponential reaching gain) can be set larger, c (sliding mode dynamic trajectory control gain) can also be set larger, while ε (constant speed reaching gain) can be smaller to reduce chattering when the system is in steady state. Thus, this paper adopts the exponential reaching law function as the applied reaching law. As known from Equation (30), i_{qs}^{*} is the output of the controller, so by setting the controller function $u=i_{qs}$, Equation (35) can be rewritten as Equation (41).

$$\dot{s}=cx_2-Du=-\varepsilon\,\mathrm{sgn}(s)-qs \tag{41}$$

The expression for the controller function u is shown as Equation (42).

$$u=\frac{1}{D}\left[cx_2+\varepsilon\,\mathrm{sgn}(s)+qs\right] \tag{42}$$

From Equation (42), the q-axis reference current can be obtained, as shown in Equation (43).

$$i_{qs}^{*}=\frac{1}{D}\int\left[cx_2+\varepsilon\,\mathrm{sgn}(s)+qs\right]dt \tag{43}$$

3.3. Feature Selection for the Motor Drive System Combining DTT and SMC

To make the control response of the BLDCM faster and more stable, the error e between the speed command and the actual speed within the motor's speed range is divided into 20 intervals (i.e., 20 states); the relationship between the intervals is shown in Figure 4. As can be seen from Figure 4, intervals Z1~Z4 have larger amplitude oscillations due to the larger gap with the speed command, while intervals Z17~Z20 have smaller speed errors, thus the amplitude oscillations are smaller. Taking the Z1 interval as an example, $e>0,\dot{e}>0$ and e is increasing; although $\dot{e}>0$, its value is decreasing, and at point m_1, $\dot{e}=0$, yet e is at its maximum. For instance, in the Z1 interval, the error e continues to increase, and the controller needs to output a higher control gain to cope with the larger error; as e approaches steady state, its control output gradually weakens.

Because the sliding mode dynamic trajectory function of the SMC has already taken the rate of change of the error $\dot{e}$ into account, the dynamic analysis diagram of Figure 3 can be simplified into 10 intervals based solely on the range of error e, to serve as the features for the DTT. The control strategy for each interval corresponds to the three variable parameters in the SMC, including the sliding mode dynamic trajectory control gain c, the exponential reaching gain q, and the constant speed reaching gain ε. However, because the constant speed reaching gain ε is not only related to the speed response but also has a decisive correlation with stability, it differs from the feature intervals of the other two. By modulating these gain values to adjust the dynamic model and reaching law function of the SMC, the transient response of the system is made faster, while simultaneously

 doi:10.20944/preprints202604.2195.v1

effectively suppressing the overshoot caused by the ERL.

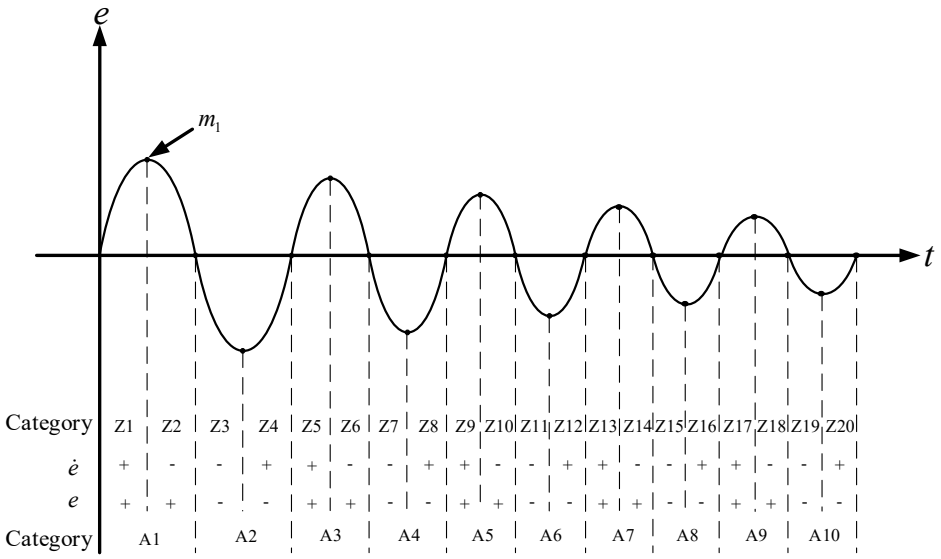

Figure 3. Dynamic analysis diagram of speed error and rate of change of speed error for the brushless DC motor.

3.4. Speed Control Combining DTT and SMC

To ensure the motor speed control response is stable and fast, this paper takes the speed error between the motor speed command and the actual speed as a feature inputted into the DTT for MSE calculation, while simultaneously completing the calculation of the sliding mode dynamic trajectory function of the SMC. First, the DTT is used to find the highest MSE reduction value ΔMSE, and it is classified as the optimal splitting point to serve as the root node of the decision tree. Then, based on this, the appropriate feature category intervals are assigned, which in turn determines the suitable three gain parameters for the SMC. The SMC adopts the ERL to enhance the response of the motor speed. Its control flow uses DTT to calculate the MSE, performs motor speed feature classification, and then determines the three gain parameters in the sliding mode dynamic trajectory function and the ERL function that can stabilize the system, so as to suppress the overshoot brought by the ERLSMC. Taking the sliding mode dynamic trajectory control gain ΔMSE as an example, the process of determining the gain parameters by the DTT is detailed as follows:

Step 1: For the corresponding feature set and the corresponding target set of each feature, construct a mathematical model as shown in Equation (44).

$$Z = \left(x_{np}, y_n\right) = \begin{bmatrix} x_{11} & x_{12} & \cdots & x_{1p} & y_1 \\ x_{21} & x_{22} & \cdots & x_{2p} & y_2 \\ \vdots & \vdots & \ddots & \vdots & \vdots \\ x_{n1} & x_{n2} & \cdots & x_{np} & y_n \end{bmatrix}, \mathrm{N} = 1,2,...,n \tag{44}$$

Where: N is the number of samples in the value range of 1 to n, and p is the number of features.

Step 2: From Equation (28), it is known that when calculating the sliding mode dynamic trajectory function s, the SMC already has a regulating and correcting effect on the rate of change of the speed error. Therefore, the rate of change of the speed error $\dot{e}$ is ignored, and only the speed error e to be classified is inputted to establish the mathematical model:

 doi:10.20944/preprints202604.2195.v1

$$Z = \begin{bmatrix} e_1 & \Delta c_1 \\ e_2 & \Delta c_2 \\ \vdots & \vdots \\ e_{10} & \Delta c_{10} \end{bmatrix}, \ N = 1,2,...,10 \tag{45}$$

Step 3: Calculate the average predicted value $\hat{y}$ from Equation (20), and substitute the calculated result into Equation (18) to obtain the initial MSE value $MSE(t)$.

Step 4: Substitute the calculated average predicted value and initial MSE value into Equation (21) to calculate the MSE reduction value ΔMSE for each node, and regard the obtained maximum value as the optimal splitting point to serve as the root node of the decision tree.

Step 5: Based on the obtained root node, split the feature set at the splitting point in a dichotomous manner to classify the category to which the speed error belongs, and determine the variation amount of the sliding mode dynamic trajectory control gain according to the assigned category. Then, recalculate the new sliding mode dynamic trajectory control gain, namely:

$$c = c_0 + \Delta c \tag{46}$$

Where: c_0 is the initial value of the sliding mode dynamic trajectory control gain, and Δc is the variation amount of the control gain.

Step 6: After judging the working condition category using the DTT, the control gain of the sliding mode dynamic trajectory in Equation (28) can be determined, which is used to alter the sliding mode dynamic trajectory function.

Step 7: Alter the sliding mode dynamic trajectory function so that the ERL does not generate excessive overshoot, and approach the sliding mode dynamic trajectory at the speed of the ERL.

Step 8: After tracking to the sliding mode dynamic trajectory, the final i_{qs}^* output is determined by Equation (43).

4. Simulation Results

The test motor in this paper uses the AM-2200H permanent magnet ELDCM [22], and its specifications are shown in Table 1. Since its rated speed is 6000rpm, the speed range is set to 0~6000rpm. Based on this, the parameters for the gain variations of each interval in Table 2 and Table 3 are determined through the aforementioned steps. Then, Matlab/Simulink is used to conduct the speed control simulation verification of the ELDCM drive system. This paper will compare the speed control performance of the ELDCM using four controllers: decision tree theory with sliding mode controller (DTTSMC), constant speed reaching law sliding mode controller (CSRLSMC), exponential reaching law sliding mode controller (ERLSMC), and extension theory with sliding mode controller (ETSMC). Among them, the ETSMC calculates the dynamic trajectory control gain of the SMC through extension theory to adjust the sliding mode dynamic trajectory function, enabling it to possess robust control performance. Figure 4(a)-(e) shows the speed command tracking responses of the BLDCM for a change of 100rpm at different speed commands (1000, 2000, 3000, 4000, 5000rpm); and Figure 5(a)-(e) shows the load regulation responses of the brushless DC motor under different speed commands (1100, 2100, 3100, 4100, 5100rpm). Among them, Figure 5(a)-(c) are the simulation results when the load change is 1N-m at speed commands (1100, 2100, 3100rpm), while Figure 5(d)-(e) are the simulation results when the load change is 2N-m at speed commands (4100, 5100rpm). From the simulation results in Figure 4 and Figure 5, it can be observed that the SMC adopting only the constant speed reaching law (CSRSMC) lacks an integral effect, so it cannot guarantee stable tracking on the speed command. In terms of load regulation response, it also requires a longer recovery time and causes an excessive speed drop. In addition, although the SMC adopting only the

 doi:10.20944/preprints202604.2195.v1

exponential reaching law (ERLSMC) has a faster response compared to the one adopting only the constant speed reaching law, overshoot occurs. Compared to the SMC adopting only the exponential reaching law (ERLSMC), the extension theory SMC (ETSMC) has a relatively fast tracking response, and the time taken for the recovery response under load changes is shorter with a smaller amplitude. However, its speed tracking response for small-amplitude changes is still insufficient, and overshoot still exists. But if the DTT is utilized to determine the three gains of the SMC, it not only effectively suppresses the overshoot brought by adopting the exponential reaching law, but also achieves better control performance in load regulation response compared to the other three.

Table 1. Specifications of the adopted ELDCM.

Electrical specifications	Electrical specifications
Three-phase rated voltage	AC 220 (V)
Three-phase rated current	AC 9.8 (A)
Rated apparent power	2156 (VA)
Rated speed	6000 (rpm)
Operating frequency range	0~2000 (Hz)
Number of poles	4
Stator resistance	0.15 (Ω)
Armature inductance	1.235e-3 (H)
Flux linkage	0.126 (Wb)
Moment of inertia	0.00145 ($kg \cdot m^2$)
Viscous friction coefficient	0.00238 ($N \cdot m \cdot s$)

Table 2. Sliding mode dynamic trajectory control gain variation Δc and exponential reaching gain variation Δq for the 10 error intervals.

Category	Error interval	Sliding mode dynamic trajectory control gain variation Δc	Exponential reaching gain variation Δq
A1	$4500 < e \leq 6000$	0	850
A2	$3000 < e \leq 4500$	0.054	1075
A3	$1500 < e \leq 3000$	2.7	1300
A4	$500 < e \leq 1500$	5.4	1400
A5	$0 < e \leq 500$	27	1500
A6	$-500 < e \leq 0$	27	1500
A7	$-1500 < e \leq -500$	5.4	1400
A8	$-3000 < e \leq -1500$	2.7	1300
A9	$-4500 < e \leq -3000$	0.054	1075
A10	$-6000 < e \leq -4500$	0	850

Table 3. SMC constant speed reaching gain variation $\Delta\varepsilon$ for the 10 error intervals.

Category	Error interval	Constant speed reaching gain variation $\Delta\varepsilon$
A1	$20 < e \leq 6000$	5000
A2	$5 < e \leq 20$	7500000
A3	$3 < e \leq 5$	500000
A4	$1 < e \leq 3$	75000
A5	$0 < e \leq 1$	500
A6	$-1 < e \leq 0$	500
A7	$-3 < e \leq -1$	75000
A8	$-5 < e \leq -3$	500000
A9	$-20 < e \leq -5$	7500000
A10	$-6000 < e \leq -20$	5000

 doi:10.20944/preprints202604.2195.v1

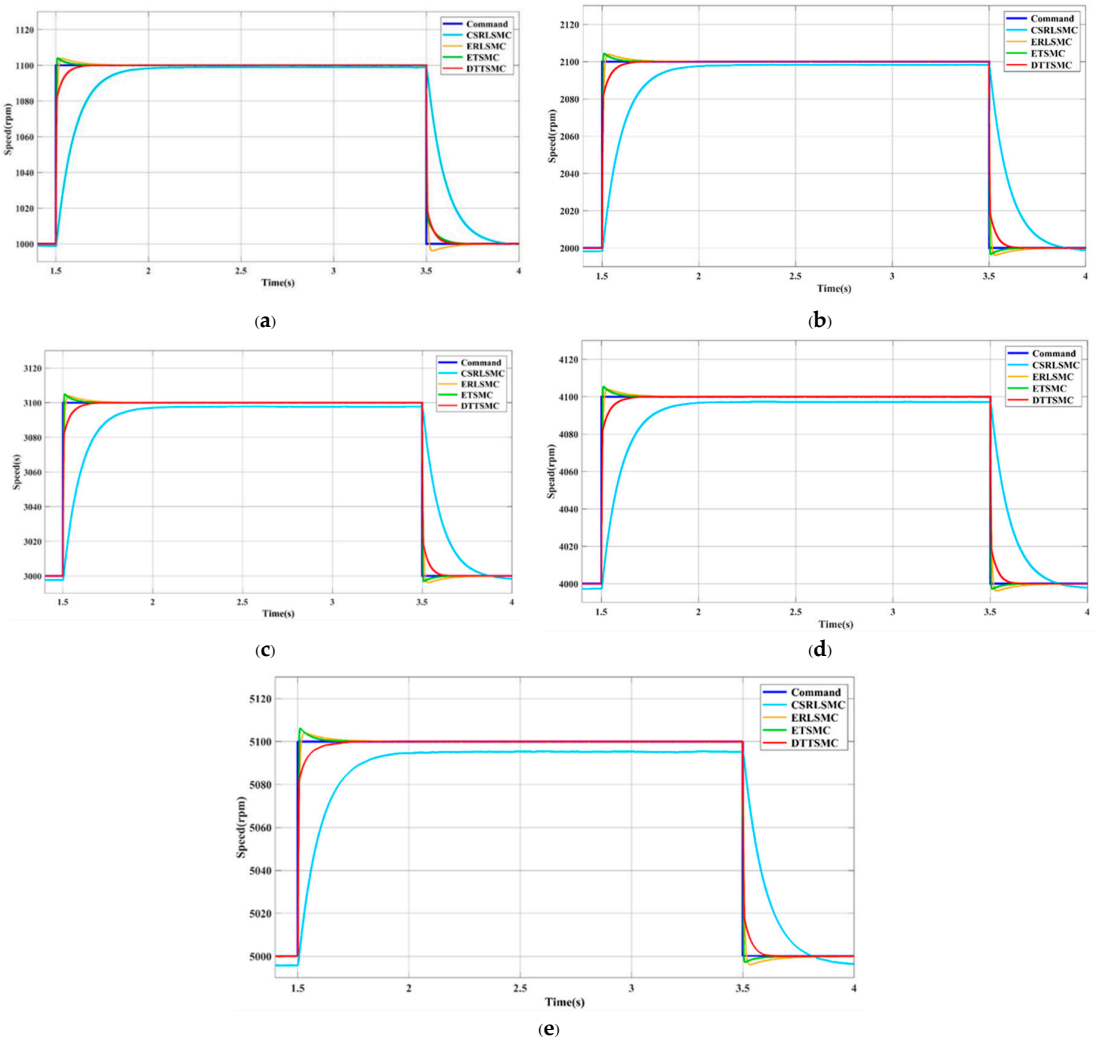

Figure 4. Comparison of tracking responses under different speed commands among the proposed DTTSMC, the CSRLSMC, the ERLSMC, and the ETSMC (The speed command increases by 100 ^{rpm} at 1.5 seconds, and returns to the original speed command at 0.35 seconds): (a)1000 → 1100 → 1000rpm,1N-m; (b)2000 → 2100 → 2000rpm,1N-m; (c)3000 → 3100 → 3000rpm, 1N-m;(d)4000 → 4100 → 4000 rpm,1N-m; (e)5000 → 5100 → 5000rpm,1N-m.

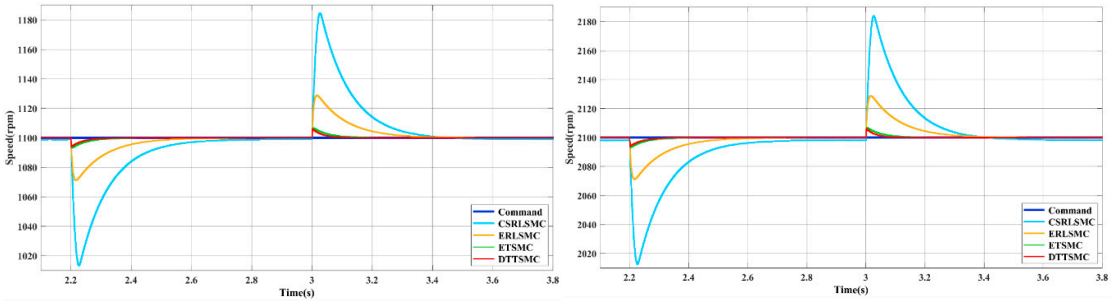

 doi:10.20944/preprints202604.2195.v1

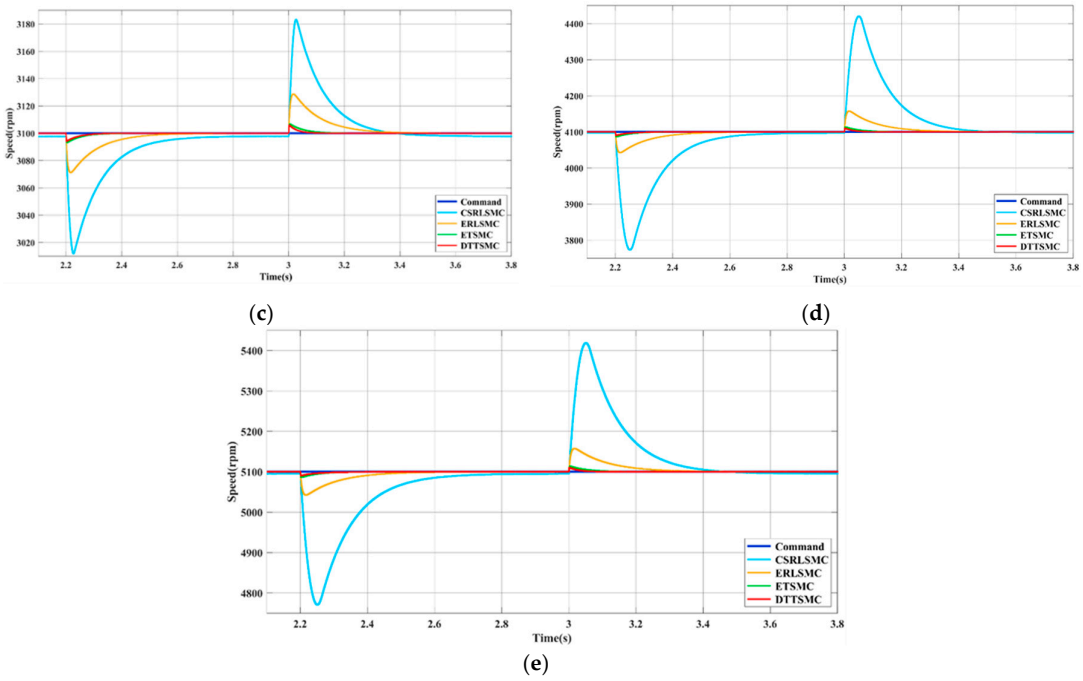

Figure 5. Comparison of load regulation responses at different speed commands among the proposed DTTSMC, the CSRLSMC, the ERLSMC, and the ETSMC (The load is applied from no-load at 2.2 seconds under different speed commands, and returns to no-load at 3 seconds): (a)1100rpm, 0 → 1 → 0N-m; (b)2100rpm, 0 → 1 → 0N-m; (c)3100rpm, 0 → 1 → 0N-m; (d)4100rpm, 0 → 2 → 0N-m; (e) 5100rpm, 0 → 2 → 0N-m.

5. Conclusions

This paper conducts speed control of a BLDCM by replacing the P-I speed controller used in traditional FOC with a control strategy combining DTT and the exponential reaching law of a SMC. The proposed novel robust controller utilizes DTT to determine the three gains of the SMC, thereby adjusting the parameters of the sliding mode dynamic trajectory function and the exponential reaching law function. This enables the BLDCM drive system under different working conditions to have a better speed tracking response compared to the CSRLSMC, the ERLSMC, and the ETSMC, allowing it to track the speed command quickly and stably. Furthermore, it possesses better control performance in load regulation response compared to the existing three improved SMCs. It not only successfully suppresses the speed overshoot caused by the SMC adopting only the exponential reaching law, but also solves the problem of slow response speed in traditional SMCs. Therefore, the proposed robust controller combining DTT and sliding mode theory with the exponential reaching law can improve performances in both speed command tracking and load regulation responses. Moreover, the proposed control law does not require massive computation or training data, making it easy to implement.

Author Contributions: K.-H.C. manages the project and completed the formal analysis of the sliding mode controller. K.-H.C. also plans the project and writes, edits and reviews the manuscript. C.-T.H. completed the formal analysis of the decision tree theory. Y.-H.G. is responsible for the software program and simulation results validation. All authors have read and agreed to the published version of the manuscript.

Funding: The authors gratefully acknowledge the support and funding of this project by the National science and Technology Council, Taiwan, under the Grant Number NSTC 114-2221-E-167-003-MY2.

Institutional Review Board Statement: Not applicable.

Informed Consent Statement: Not applicable.

 doi:10.20944/preprints202604.2195.v1

Data Availability Statement: This study did not report any data.

Conflicts of Interest: The authors of the manuscript declare no conflicts of interest.

Nomenclature:

Acronyms

BLDCM	:	brushless DC motor
FOC	:	field-oriented control
DTT	:	decision tree theory
SMT	:	sliding mode theory
CART	:	classification and regression tree
ERLSMC	:	exponential reaching law sliding mode controller
MSE	:	mean squared error
ERL	:	exponential reaching law
CSRL	:	constant speed reaching law
ETERL	:	extension theory combined with exponential reaching law
P-I	:	proportional-integral
FLT	:	fuzzy logic theory
ET	:	extension theory
2DOFC	:	two-degree-of-freedom controller
SVPWM	:	space vector pulse width modulation
MTPA	:	maximum torque per ampere
MAE	:	mean absolute error
SMC	:	sliding mode controller
DTTSMC	:	decision tree theory with sliding mode controller
CSRLSMC	:	constant speed reaching law sliding mode controller

Symbols

ϕ_{ds}, ϕ_{qs}	:	stator fluxes of the d-axis and q-axis
ϕ_F	:	flux linkage
v_{ds}, v_{qs}	:	stator voltages of the d-axis and q-axis
R_s	:	stator resistance
i_{ds}, i_{qs}	:	stator currents of the d-axis and q-axis
ω_e	:	electrical angular velocity
L_d, L_q	:	stator inductances of the d-axis and q-axis
T_e	:	electromagnetic torque
P	:	number of poles
J	:	moment of inertia
ω_m	:	mechanical rotational speed
T_L	:	load torque
J	:	moment of inertia
p_i	:	proportion of the i-th category in node t
C_n	:	number of categories
t_{left}, t_{right}	:	left child node and right child node
N	:	number of samples in node t
N_{left}, N_{right}	:	number of samples in the left and right child nodes
y_i	:	actual value of sample i
$\hat{y}$	:	sample mean in the node (i.e., the average predicted value)
s	:	sliding line function
c	:	sliding line control gain
x_1, x_2	:	state variable functions
$\dot{s}$	:	reaching law function
ε	:	constant speed reaching gain
q	:	exponential reaching gain

 doi:10.20944/preprints202604.2195.v1

$\mathrm{sgn}(s)$	: sign function
C	: constant of integration
N	: number of samples in the value range of 1 to n
p	: number of features
c_0	: initial value of the sliding mode dynamic trajectory control gain
Δc	: variation amount of the control gain

References

1. Wang, M.; Chen, Z. Research on Permanent Magnet Structure of Permanent Magnet Synchronous Motor for Electric Vehicle. In Proceedings of the 2nd International Conference on Electrical Engineering and Control Science (IC2ECS), Nanjing, China, 16–18 December 2022; pp.990–993.
2. Lee, C. I.; Jang, G. H. Experimental Measurement and Simulated Verification of the Unbalanced Magnetic Force in Brushless DC Motors. *IEEE Trans. Magnt*. **2008**, 44, 4377–4380.
3. BV, P.; Balamurugan, A.; Selvathai, T.; Reginald, R.; Varadhan, J. Evaluation of Different Vector Control Methods for Electric Vehicle Application. In Proceedings of the 2nd International Conference on Power and Embedded Drive Control (ICPEDC), Chennai, India, 21–23 August 2019; pp. 273–278.
4. Bhatti, S. A.; Malik, S. A.; Daraz, A. Comparison of P-I and I-P controller by Using Ziegler-Nichols Tuning Method for Speed Control of DC Motor. In Proceedings of the International Conference on Intelligent Systems Engineering (ICISE), Islamabad, Pakistan, 15–17 January 2016; pp. 1–5.
5. Murali, S. B.; Rao, P. M. Adaptive Sliding Mode Control of BLDC Motor Using Cuckoo Search Algorithm. In Proceedings of the 2nd International Conference on Inventive Systems and Control (ICISC), Coimbatore, India, 19–20 January 2018; pp. 989–993.
6. Qi, C.; Xie, J.; Mao, H.; Xie, Q. Condition Assessment of Valve-side Bushing of Converter Transformer Based on Extension Theory. In Proceedings of the IEEE International Conference on High Voltage Engineering and Application (ICHVE), Beijing, China, 06–10 September 2020; pp. 1–6.
7. Wu, H. Q.; Chen, Y. W.; Liu, R. College Education Outcome Expectation and Proactive Personality as Predictors of Chinese College Students' Learning Motivation, Career Adaptability as a Mediator. In Proceedings of the International Conference on Modern Education and Information Management (ICMEIM), Dalian, China, 25–27 September 2020; pp. 716–721.
8. Lu, S.; Tang, X.; Song, B.; Zhou, B. An Optimal Fuzzy-PI Controller for the High-Performance Speed Control of a PMSM. In Proceedings of the 2nd International Conference on Instrumentation, Measurement, Computer, Communication and Control, Harbin, China, 08–10 December 2012; pp. 1503–1507.
9. Chao, K. H.; Hsieh, C. T.; Chen, X. J. A Robust Controller Based on Extension Sliding Mode Theory for Brushless DC Motor Drives. *Electronics*, **2024,** 13, 4028, 1–26.
10. Chao, K. H.; Chang, C. L. Design of a Robust Controller for Induction Motor Drive Systems Based on Extendable Fuzzy Theory. *Mathematics*, **2024,** 12, 3235, 1–20.
11. Wang, J.; Ye, J.; Yan, R. The Magnetostatic Simulation and Determination of Magnetic Components for an External Ventricular Drainage Device. In Proceedings of the 40th Chinese Control Conference (CCC), Shanghai, China, 26–28 July 2021; pp. 6386–6391.
12. Xie, T.; Kuai, Z.; Ye, X.; Zhu, L.; Guo, K.; Shi, S. Coordinate Conversions and Deviation Analysis in Multi-source Data Fusion. In Proceedings of the 2nd China International SAR Symposium (CISS), Shanghai, China, 03–05 November 2021; pp. 1–3.
13. Liu, C. H. *AC Motor Control: The Principles of Vector Control and Direct Torque Control*, 4th ed.; Tonghua Books Co., Ltd.: Taipei, Taiwan, 2007; pp. 33–217.
14. Kishore, N.; Shukla, K.; Gupta, N. A Novel Three-phase Multilevel Inverter Cascaded by Three-phase Two-level Inverter and Two Single-phase Boosted H-bridge Inverters. In Proceedings of the IEEE PES Innovative Smart Grid Technologies-Asia (ISGT Asia), Singapore, Singapore, 01–05 November 2022; pp. 330–334.
15. Butt, C.; Hoque, M. A.; Rahman, M. A. Simplified Fuzzy Logic Based MTPA Speed Control of IPMSM Drive. In Proceedings of the 38th IAS Annual Meeting on Conference Record of the Industry Applications Conference, Salt Lake City, UT, USA, 12–16 October 2003; pp. 499–506.

 doi:10.20944/preprints202604.2195.v1

16. Luo, N.; Zhang, L. Chaos Driven Development for Software Robustness Enhancement. In Proceedings of the 9th International Conference on Dependable Systems and Their Applications (DSA), Wulumuqi, China, 04–05 August 2022; pp. 1029–1034.
17. Sun, J.; Jiang, N.; Sun, G.; Huang, W. Analysis of CART Algorithms in Data Mining. In Proceedings of the 2nd International Conference on Machine Learning, Cloud Computing and Intelligent Mining (MLCCIM), Jiuzhaigou, China, 25–29 July 2023; pp. 548–553.
18. Xie, H.; Shang. F. The Study of Methods for Post-pruning Decision Trees Based on Comprehensive Evaluation Standard. In Proceedings of the 11th International Conference on Fuzzy Systems and Knowledge Discovery (FSKD), Xiamen, China, 19–21 August 2014; pp. 903–908.
19. Variable Structure Control System. Available Online: https://www.youtube.com/watch?v=vc76WZ0AQcY&list=PLj6E8qlqmkFuIY_c3QvyBFTBiWhqN1Fm0&ab_channel=NYCUOCW (accessed on December 2024).
20. Zhang, J.; Liu, B.; Jiang, Z.; Hu, H. The Application of Sliding Mode Control with Improved Approaching Law in Manipulator Control. In Proceedings of the 13th IEEE Conference on Industrial Electronics and Applications (ICIEA), Wuhan, China, 31 May–02 June 2018; pp. 807–812.
21. Bodur, F.; Kaplan, O. A Novel Sliding Mode Control Based on Super Twisting Reaching Law for PMSM Speed Controller with Fixed-time Disturbance Observer. In Proceedings of the 12th International Conference on Renewable Energy Research and Applications (ICRERA), Oshawa, ON, Canada, 29 August–01 September 2023; pp. 563–568.
22. The AM2200H BLDC Motor Supply Produced by Adlee Powertronic Co., Ltd. Available Online: https://www.adlee.com/zh-tw/product-552515/%E5%B7%A5%E6%A5%AD%E7%94%A8%E7%9B%B4%E6%B5%81%E7%84%A1%E5%88%B7%E9%A6% AC%E9%81%94.html (accessed on December 2024).